Available online at www.sciencedirect.com
ScienceDirect
Journal of the European Ceramic Society 30 (2010) 335–339
www.elsevier.com/locate/jeurceramsoc

Raman spectra and extended X-ray absorption fine structure characterization of $La_{(2-x)/3}Na_xTiO_3$ and $Nd_{(2-x)/3}Li_xTiO_3$ microwave ceramics

Mei-Yu Chen [a], Ching Yu Chiu [a], Chia-Ta Chia [a,*], J.F. Lee [b], J.J. Bian [c]

[a] *Department of Physics, National Taiwan Normal University, Taipei 116, Taiwan*
[b] *National Synchrotron Radiation Research Center, Hsinchu 300, Taiwan*
[c] *Department of Inorganic Materials, Shanghai University, 149 YanChang Road, Zhabei District, Shanghai 200072, People's Republic of China*

Available online 15 August 2009

Abstract

A-site deficient perovskite compounds, $La_{(2-x)/3}Na_xTiO_3$ ($0.02 \le x \le 0.5$) and $Nd_{(2-x)/3}Li_xTiO_3$ ($0.1 \le x \le 0.5$) microwave ceramics, were investigated by Raman scattering. $Nd_{(2-x)/3}Li_xTiO_3$ ($0.1 \le x \le 0.5$) was also investigated by extended X-ray absorption fine structure (EXAFS) measurement. The Raman shifts of the E ($239\,cm^{-1}$) and A_1 ($322\,cm^{-1}$) modes of $La_{(2-x)/3}Na_xTiO_3$ were found to decrease with x. However, the E ($254\,cm^{-1}$) and A_1 ($338\,cm^{-1}$) of $Nd_{(2-x)/3}Li_xTiO_3$ were found to blueshift with x, which was caused by Li substitution. The redshift of the A_1 ($471\,cm^{-1}$) phonon of $Nd_{(2-x)/3}Li_xTiO_3$ ($0.1 \le x \le 0.3$) indicates that O–Ti–O bonding forces lessen with Li concentration, which is consistent with the EXAFS result that Ti–O bond lengths increase for $0.1 \le x \le 0.3$. For $x > 0.3$, the EXAFS result shows that Ti–O bond lengths decrease. Moreover, Ti–O bond lengths show strong correlation with the microwave dielectric constants of $Nd_{(2-x)/3}Li_xTiO_3$.

Keywords: Dielectric properties; X-ray methods; Spectroscopy; Optical properties

1. Introduction

In previous years, many perovskite-type structures with a general formula of ABO_3 have been studied because their superior optic, magnetic, and electric properties are advantageous to technical applications such as mobile phones and satellite systems. The prototype perovskite structure has a cubic structure of the space group $Pm3m$ (O_h^1, $Z = 1$). Many complex perovskite-like materials are derived from a general ABO_3 perovskite family replacing A or B cations from different compounds such as $A(B_{1/2}'B_{1/2}'')O_3$, $A\,(B_{1/3}'B_{2/3}'')O_3$, $(A_{1/2}'A_{1/2}'')BO_3$, and $(A_{1/2}'A_{1/2}'')(B_{1/2}'B_{1/2}'')O_3$.

Lanthanum titanate ($La_{2/3}TiO_3$)-based perovskite compounds which have one-third A-site vacancies possess excellent microwave dielectric properties. However, it is difficult to obtain pure $La_{2/3}TiO_3$ because of its high A-site vacancies. For this reason, the structure can be stabilized by inserting low-concentration substitutions on the A-site and B-site, or by compensating for the oxygen deficiency.[1–6]

It has been reported that the orthorhombic structures of ($La_{2/3}TiO_3$)-based perovskite display an ordering arrangement of A-site cations, and their unit cells transform to double sizes along each direction.[3] The A-site cations ordering is comprised $z = 0$ layers fully occupied by La^{3+} ions and $z = 1/2$ layers, which are in turn occupied by vacancies and La^{3+} ions. Kim et al. and Yoshii revealed that the structure of $La_{2/3}TiO_3$ and $Nd_{2/3}TiO_3$ systems are of orthorhombic *Pmmm* symmetry.[2,7] MacEachern et al. showed the orthorhombic *Pban* symmetry of $La_{2/3}TiO_3$, which shows $\sqrt{2}a_p \times \sqrt{2}a_p \times 2a_p$ cell by neutron diffraction.[8] There are many controversial results which were found through several different techniques such as the use of insertion ions and the sintered method. More recently, precision measurement was made to demonstrate that the crystal symmetry of $La_{2/3}TiO_3$ and $Nd_{2/3}TiO_3$ is orthorhombic *Cmmm*.[1,4,6,9]

Doping Li^+ ion into $La_{2/3}TiO_3$ and $Nd_{2/3}TiO_3$ compounds results in high ionic conductivity, which can applied to solid oxide fuel cells (SOFC) and other electrodevices.[10–15] Meanwhile, substituting Na^+ ions in $La_{2/3}TiO_3$ has been much less studied. Ruiz et al. investigated the structure of the $La_{1.33-x}Na_{3x}Ti_2O_6$ series via neutron diffraction and electron microscopy techniques.[16] Through these measurements, the $x = 0.11$ sample was found to display *Cmmm* orthorhombic

* Corresponding author. Tel.: +886 2 29346620x115; fax: +886 2 29346408.
E-mail address: chiact@ntnu.edu.tw (C.-T. Chia).

0955-2219/$ – see front matter © 2009 Elsevier Ltd. All rights reserved.
doi:10.1016/j.jeurceramsoc.2009.07.024

structure, while $x = 0.16$ and $x = 0.25$ display *Pbmm* and *Ibmm* orthorhombic structures on $\sqrt{2}a_p \times \sqrt{2}a_p \times 2a_p$ cells, respectively. A-site ordering has been built by one layer of La atoms and one layer of La/Na/vacancies along the *c*-axis, while the layer of La/Na/vacancies is fully occupied or half occupied. Titanium atoms would move from their ideal sites toward the Na/vacancies layer in a low sodium concentration. The $Nd_{0.5}Li_{0.5}TiO_3$ structure shows tetragonal symmetry of the space group *P*-4*b*2, which was refined by X-ray and neutron diffraction.

Inserting different ions to A-site vacancies would affect the A-site ordering and oxygen octahedra of the B-site. Raman measurement is one of the best tools for this because it is uncontacted, undestroyed, and sensitive for detecting the local structure of microwave materials. In this work, the Raman technique will be utilized to investigate the microstructure of $La_{(2-x)/3}Li_xTiO_3$ and $La_{0.5}(Li,Na)_{0.5}TiO_3$ compounds.[18,19] Based on the analysis of the group theory, the Raman active phonon modes of two series compounds could be proven. The BO_6 local octahedra structure of $Nd_{(2-x)/3}Li_xTiO_3$ would be detected by the extended X-ray absorption fine structure (EXAFS) technique. Furthermore, it could be predicted that the microstructure has a close correlation with microwave dielectric properties.

2. Experiment

The polycrystalline of $La_{(2-x)/3}Na_xTiO_3$ with $0.02 \le x \le 0.5$ and $Nd_{(2-x)/3}Li_xTiO_3$ with $0 \le x \le 0.5$ samples was studied by the group of Bian et al. at Shanghai University.[11,20] $La_{(2-x)/3}Na_xTiO_3$ was prepared using the conventional solid-state reaction process, which includes the starting materials TiO_2 (99.99%), $NaCO_3$ (99.99%), and La_2O_3 (99.99%). These oxide compounds were weighed and mixed with ZrO_2 balls in ethanol for 24 h, then dried and calcined at 1100 °C for 2 h in alumina crucible. These calcined powders were ground, dried, and mixed with 7 wt.% PVA. The mixtures were then pressed into pellets. The compounds were sintered at 1400 °C for 2 h. Similarly, $Nd_{(2-x)/3}Li_xTiO_3$ was prepared from starting materials including TiO_2 (99.99%), $LiCO_3$ (99.99%), and Nd_2O_3 (99.99%). They were calcined at 1100 °C for 2 h and sintered at 1300 °C for another 2 h. The microwave dielectric properties were measured using HP 8720C network analyzer, between 7 and 8 GHz, and the TE_{011} resonant cavity method. Raman spectra were measured at room temperature and recorded using JOBIN IVON T6400 triple-grating Raman spectrometer equipped with liquid-nitrogen-cooled CCD. The 10 mW output of the 514.5 nm line of Ar^+ laser was used as the excitation source. The obtained Raman spectra exhibited the resolution of approximately 0.6 cm^{-1}. The titanium K-edge core EXAFS experiment of $Nd_{(2-x)/3}Li_xTiO_3$ was measured via fluorescence mode in wiggler beamline BL17C at the National Synchrotron Radiation Research Center of Taiwan. The structural parameters of TiO_6 were examined using the FEFF-8 code.

3. Results and discussion

In recent years, Ruiz et al. have made many discoveries about the structure identification of $La_{1.33-x}M_{3x}Ti_2O_6$ (M = Li, Na, K) through neutron powder diffraction, X-ray powder diffraction, and the Scanning electron microscopy (SEM) technique. The crystal structure of $La_{(2-x)/3}Na_xTiO_3$ was characterized as *Cmmm* symmetry when $x \le 0.2$, and *Ibmm* symmetry when $x \ge 0.2$.[16,20] A similar compound, $Nd_{(2-x)/3}Li_xTiO_3$, was also studied.[9,17] With Li^+ ion concentration, the phase of $Nd_{(2-x)/3}Li_xTiO_3$ can be altered from *Cmmm* symmetry to *P*-4*b*2 (D^7_{2d}) symmetry.

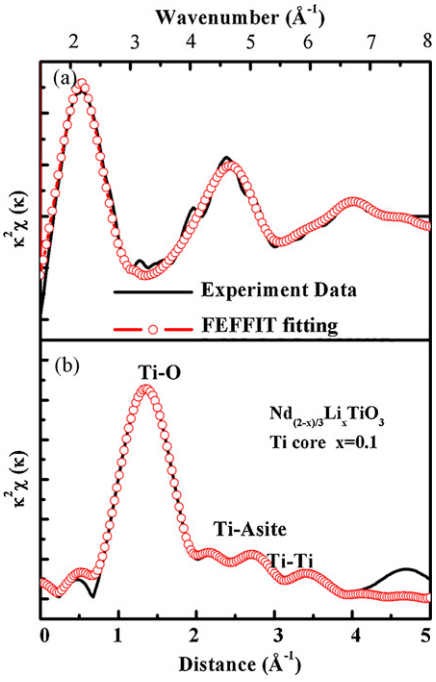

Fig. 1. FEFFIT result of the EXAFS signal for $Nd_{(2-x)/3}Li_xTiO_3$. (a) k^2 weighted EXAFS signal of the Ti K-edge in *k* space and (b) in *R* space.

The EXAFS experiment on $La_{(2-x)/3}Na_xTiO_3$ cannot be conducted because the L_{III}-edge energy of La (5483 eV) is close to the K-edge (4966 eV) energy of the Ti atom. However, it is fortunate that the local TiO_6 structure of $Nd_{(2-x)/3}Li_xTiO_3$ can be investigated by EXAFS experiment. Utilizing the AUTOBK program to remove the backgrounds of the curves as shown in Fig. 1(a), the absorbance oscillation caused by the backscattering of Ti atom's surrounding atoms can be obtained. Fig. 1(a) shows the *k*-weighted $[k^2\chi(k)]$ EXAFS signals of the Ti core atoms at the range of 2–7.2 $Å^{-1}$ in wavenumber space. Fig. 1(b) shows the Fourier transformation of the *k*-weighted $[k^2\chi(k)]$ EXAFS signals. To deduce the structural parameters of TiO_6, the FEFF-8.2 program calculates the backscattering interference paths in the 2–7.2 Å region. In Fig. 1, the solid lines represent the experimental data, while the hollow lines represent the fitting curves. The *R*-factors of fitting are all below 0.002. From Fig. 1(b), the first peak is attributed to the six oxygen atoms which form an oxygen octahedron.

Fig. 2 shows the correlation between the average bond distance of Ti–O and the dielectric constant with Li concentration. Apparently, the size of TiO_6 increases from $x = 0.1$ to 0.3. Beyond $x = 0.3$ concentration, the size of TiO_6 becomes smaller. For a low Li concentration, the result could be interpreted as the increase in Li^+ ions. With an increase in Li^+ ions, the oxygen

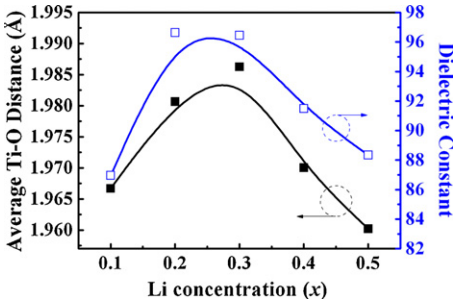

Fig. 2. Correlation of the average Ti–O bond length and dielectric constant.

atoms would be attracted toward the A-site, and thus the Ti–O distance would increase. However, at a high Li concentration ($x > 0.3$), the average polarizability of the A-site diminishes due to the small polarizability of Li. To maintain the charge balance of the local structure, three Li^+ ions are needed to compensate for one $Nd3^+$ ion. The average polarizability of $La_{(2-x)/3}Na_xTiO_3$ changes from 5.01 to 3.6 (1.2×3). This would cause the decrease in attraction between the A-site and the oxygen atoms, making the Ti–O distance decrease. The size variation of oxygen octahedra would affect microwave dielectric performance.

Fig. 3(a) shows the Raman spectra of $La_{(2-x)/3}Na_xTiO_3$ at room temperature. The lineshapes around the low-frequency region obviously show different patterns above $x = 0.3$. Phase transition exists in two end members of $La_{(2-x)/3}Na_xTiO_3$, which are determined by XRD and Raman spectra. Similarly, Fig. 3(b) shows the Raman spectra of the $Nd_{(2-x)/3}Li_xTiO_3$ samples, as well as demonstrates the phase transitions found for $x \geq 0.3$.

The orthorhombic $La_{(2-x)/3}Na_xTiO_3$ in the region $0.02 \leq x \leq 0.2$ show the symmetry of *Cmmm* ($Z = 4$) with a Glazer notation of $a^0b^-c^0$. The 60 Raman active modes, "$18A_g + 14B_{1g} + 16B_{2g} + 14B_{3g}$," were obtained from factor group analysis. The 12, 12, and 36 Raman active modes are contributed to the vibrations of A-site cations, Ti^{4+} ion, and O^{2-} ions, respectively. However, these Raman spectra display much fewer phonons than the calculated ones because various peaks might overlap with one another. In addition, when the doping concentration in $0.3 \leq x \leq 0.5$, the group theory deduces that structures exhibit *Ibmm* ($Z = 4$) symmetry, $a^-b^0c^-$ of Glazer notation, and 24 Raman active modes that could be produced as "$6A_g + 4B_{1g} + 6B_{2g} + 8B_{3g}$."

Similarly, the orthorhombic $0.1 \leq x \leq 0.3$ of the $Nd_{(2-x)/3}Li_xTiO_3$ samples show the symmetry of *Cmmm* ($Z = 4$) with a Glazer notation of $a^0b^-c^0$. Sixty Raman active modes could be calculated, and these modes had the same result with $0.02 \leq x \leq 0.2$ of the $La_{(2-x)/3}Na_xTiO_3$ samples. For $x = 0.4$ and 0.5 of $Nd_{(2-x)/3}Li_xTiO_3$, the group theory deduces that the structures exhibit *P*-4*b*2 ($Z = 4$) with a Glazer notation of $a^0a^0c^-$, and 30 Raman active modes could be produced as "$4A_1 + 6B_1 + 7B_2 + 17E$."

The symmetry of *Cmmm*, *Ibmm*, and *P*-4*b*2 could be derived from the undistorted *Pm3m* structure ABO_3 by the distortion of the BO_6 oxygen octahedral and the replacement of cations. The Raman spectra of $La_{(2-x)/3}Na_xTiO_3$ ($x = 0.02$, 0.04, 0.06, 0.1, 0.2) and $Nd_{(2-x)/3}Li_xTiO_3$ ($x = 0.1$, 0.2, 0.3) were measured at room temperature in Fig. 3(a) and (b) and were analyzed using the 20 and 19 Lorentz-model function to discuss the lineshift and width of the main phonons, respectively.[18] These modes of two series compounds are analyzed by three parts as follows: numbers in brackets represent the modes of $Nd_{(2-x)/3}Li_xTiO_3$. (i). There are three main phonons in the lowest frequencies: the 113 (105) cm^{-1} and 143 (141) cm^{-1} peaks are akin to the Ti displacement in the *x*–*y* plane of the E_g modes of $BaTiO_3$, and the 161 (164) cm^{-1} peak corresponds to the A-site displacement of the A_1 symmetry of $BaTiO_3$. (ii) The phonons in the 200–400 cm^{-1} region are all associated with A-site cation displacement: the 239 (254) cm^{-1} peak resembles the E mode of PbTiO3, and the 322 (338) cm^{-1} peak corresponds to the A_1 mode of $PbTiO_3$. (iii) The phonons in high-frequency regions contribute to oxygen movement: the 461 (471) cm^{-1} peak corresponds to O–Ti–O displacement along the *z*-axis of the A_1 mode of $PbTiO_3$; the 526 (524) cm^{-1} peak is analogous to the E mode; 563 and 588 (553 and 592) cm^{-1} belong to the A_1 mode; and the broad phonons in 650–1000 cm^{-1} are related to oxygen octahedral stretching vibration.

Obviously, the phonon widths of $La_{(2-x)/3}Na_xTiO_3$ are widened with an increase in sodium concentration. In Fig. 4(a), the width of the E (143 cm^{-1}) mode was plotted versus the sodium concentration for $La_{(2-x)/3}Na_xTiO_3$, as well as the correlation between the widths and $Q \times f$ value. The wider phonon width gives a shorter phonon lifetime, and it indicates a higher power consumption for microwave propagation, therefore a smaller $Q \times f$ value is expected. Due to A-site ordering, oxygen octahedral distortion, impurity, and other factors, the widths of $La_{(2-x)/3}Na_xTiO_3$ below $x = 0.08$ cannot fully match this status. In addition, Fig. 4(b) describes the relationship between the width of E (141 cm^{-1}) mode and the $Q \times f$

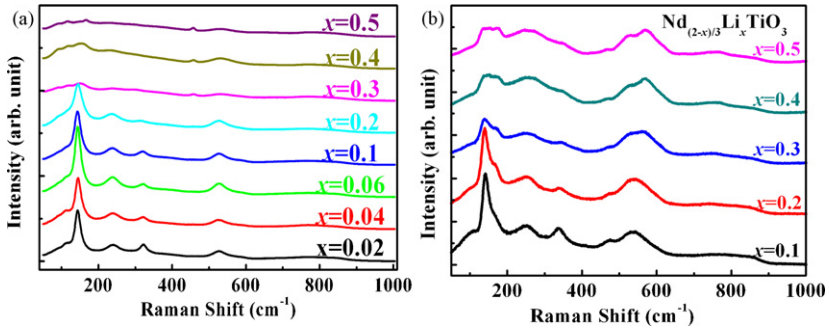

Fig. 3. The Raman Spectra of the $La_{(2-x)3}Na_xTiO_3$ materials with $0.02 \leq x \leq 0.5$ and (b) $Nd_{(2-x)3}Li_xTiO_3$ materials with $0.1 \leq x \leq 0.5$.

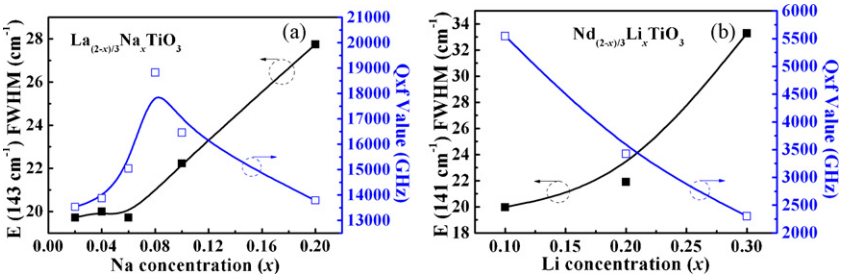

Fig. 4. Correlation of the E (143 and 141 cm^{-1}) mode FWHM and the $Q \times f$ value for (a) $La_{(2-x)/3}Na_xTiO_3$ (b) $Nd_{(2-x)/3}Li_xTiO_3$.

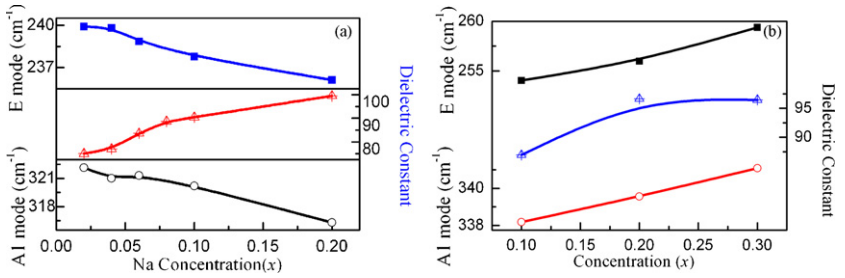

Fig. 5. Correlation of the A1 and E modes of Raman shift with the dielectric constant for the (a) $La_{(2-x)/3}Na_xTiO_3$ (b) $Nd_{(2-x)/3}Li_xTiO_3$.

value of $Nd_{(2-x)/3}Li_xTiO_3$ with lithium concentration. The width and $Q \times f$ value exhibit an inverse correlation when the lithium content increases, which is shown in Fig. 4(b).

Fig. 5(a) and (b) characterizes the properties of the E (233 and 254 cm^{-1}) mode and A_1 (318 and 339 cm^{-1}) mode of $La_{(2-x)/3}Na_xTiO_3$ and $Nd_{(2-x)/3}Li_xTiO_3$. The correlation between the Raman shifts and the dielectric constants can be observed in Fig. 5(a) and (b). When the Raman shift of the E (254 cm^{-1}) and A_1 (318 cm^{-1}) mode of $La_{(2-x)/3}Na_xTiO_3$ decreases, their dielectric constant tends to become larger. However, the Raman results of $Nd_{(2-x)/3}Li_xTiO_3$ relatively show the trend to become larger numbers regardless of the phonon frequency or their dielectric constant.

Theoretically, one of the predominant factors that influence Raman shift is the force constant k which is proportional to vibration frequency. In general, a weaker crystal structure displays a larger dielectric constant and smaller force constant, while the Raman shift usually shows redshift phenomenon. The Raman results of $La_{(2-x)/3}Na_xTiO_3$ from Fig. 5 are consistent with this status. However, the Raman results of $Nd_{(2-x)/3}Li_xTiO_3$ do not behave according to this hypothesis. The reason is that reduced mass is another dominant factor that must be considered. For the E and A_1 modes of two series samples, the vibration modes belong to a relative motion between A-site cations and TiO_6 octahedra. In the $Nd_{(2-x)/3}Li_xTiO_3$ case, due to Li doping, the reduced mass of the A-site declines substantially. The mass of lithium (6.94 amu) is much lighter than that of neodymium (144 amu). The mass decay rate is so fierce that the Raman shift of A_1 and E shows an upward tendency even though the dielectric constant rises due to Li doping. On the other hand, for $La_{(2-x)/3}Na_xTiO_3$, the mass of lanthanum is 139 amu, and that of sodium is 24.0 amu The mass decay slope of $La_{(2-x)/3}Na_xTiO_3$ becomes smoother. To summarize the two factors that affect frequency, the dominant factor that affects the frequency of $La_{(2-x)/3}Na_xTiO_3$ is the force constant k, which could be reflected by the microwave dielectric constant. In contrast, the determinant factor that influences the Raman shift of $Nd_{(2-x)/3}Li_xTiO_3$ is the decay speed of reduced mass.

The A_1 (461 cm^{-1}) mode of $La_{(2-x)/3}Na_xTiO_3$ cannot been found for x<0.2, but that (471 cm^{-1}) of $Nd_{(2-x)/3}Li_xTiO_3$ can been obviously seen. Fig. 6 clearly reveals the correlation between the Raman shift of the A_1 mode of $Nd_{(2-x)/3}Li_xTiO_3$ and the dielectric constant in the microwave region. The Raman shift of the A_1 (471 cm^{-1}) mode decreases with Li concentration, while the A_1 mode represents O–Ti–O displacement along the z-axis. It is obvious that the bonding forces between two oxygen atoms and titanium become smaller, which would cause the results of the $Nd_{(2-x)/3}Li_xTiO_3$ dielectric constant to increase along with the lithium concentration. This fact is consistent with the EXAFS results of $Nd_{(2-x)/3}Li_xTiO_3$.

The A_1 (563 and 588 cm^{-1}) modes of the $La_{(2-x)/3}Na_xTiO_3$ series represent the orbital oxygen movement along the z-axis. The intensities of the A_1 (563 and 588 cm^{-1}) modes in the $La_{(2-x)/3}Na_xTiO_3$ spectra are not apparent as shown in Fig. 3(a), but the intensities of the A_1 (553 and 592 cm^{-1})

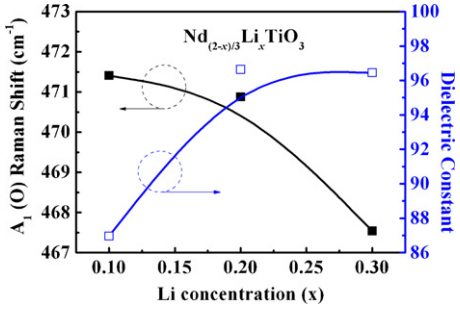

Fig. 6. Correlation between Raman shift and the dielectric constant for A_1 (471 cm^{-1}) in $Nd_{(2-x)/3}Li_xTiO_3$.

modes in the $Nd_{(2-x)/3}Li_xTiO_3$ spectra are easy to observe as shown in Fig. 3(b). Therefore, it shows that lithium doping has strongly influenced on A_1 modes' characteristics of the $Nd_{(2-x)/3}Li_xTiO_3$. This result is similar to that in a study of $La_{0.5}(Li,Na)_{0.5}TiO_3$ by Sanjuán et al.[19] Sanjuán et al. show the results that the intensities of A_1 modes increase with larger lithium content and with less sodium content. From the 650 to 1000 cm^{-1} region, the characteristic of the broad phonon due to the stretching vibration of TiO_6 octahedra was found to have no significant change caused by either lithium and sodium substitution.

4. Conclusion

In this paper, two series of $La_{(2-x)/3}Na_xTiO_3$ and $Nd_{(2-x)/3}Li_xTiO_3$ materials were studied by Raman scattering and extended X-ray absorption fine structure measurement at room temperature. The Raman and EXAFS experiments exhibit high sensitivity to microstructure variation, so the close correlation with microwave dielectric properties, the phonon's characteristics, and the microstructure features were correspondingly discussed. The Raman spectra and X-ray diffraction provide evidence to affirm that the phase transition took place from *Cmmm* to *Ibmm* at $0.2 \leq x \leq 0.3$ of $La_{(2-x)/3}Na_xTiO_3$, and from *Cmmm* to *P*-4*b*2 at $x = 0.3$ of $Nd_{(2-x)/3}Li_xTiO_3$, respectively. All phonons of the Raman spectra broadened, and the *Qxf* values decreased with an increase in the substitution rate ($x > 10\%$) regardless of $La_{(2-x)/3}Na_xTiO_3$ or $Nd_{(2-x)/3}Li_xTiO_3$. The E (233, 254 cm^{-1}) and A_1 (322, 338 cm^{-1}) modes tend to redshift for the $La_{(2-x)/3}Na_xTiO_3$ series, but these two modes blueshift for the $Nd_{(2-x)/3}Li_xTiO_3$ samples due to the insertion of small size of lithium atom. The dominant factors that cause this interesting result are the decline rate of the reduced mass and the increasing dielectric constant. The A_1 (471 cm^{-1}) modes of $Nd_{(2-x)/3}Li_xTiO_3$, which have been identified as O–Ti–O vibration along the *z*-axis, show the redshift tendency due to Li doping. From the EXAFS results for $Nd_{(2-x)/3}Li_xTiO_3$, the average distances of Ti–O and O–Ti–O along the *z*-axis both increase in the $x \leq 0.3$ region. It can be shown that the volumes of TiO_6 are proportional to their microwave dielectric constant. The EXAFS results are consistent with the Raman findings of the A_1 (471 cm^{-1}) phonon of $Nd_{(2-x)/3}Li_xTiO_3$. Therefore, it proves that the microstructures of $La_{(2-x)/3}Na_xTiO_3$ and $Nd_{(2-x)/3}Li_xTiO_3$ show high correlation with microwave dielectric properties.

Acknowledgement

The authors would like to thank the National Science Council of the Republic of China for financially supporting this research under Contract Nos. NSC 96-2112-M-003-009-MY3 and NSC 97-2627-M-003-003.

References

1. Howard, C. J. and Zang, Z., Structures and phase transition in the layered perovskite $La_{0.6}Sr_{0.1}TiO_3$: a new orthorhombic structure solved from high-resolution diffraction in combination with group theoretical analysis. *J. Phys. Condens. Matter.*, 2003, **15**, 4543–4553.
2. Kim, I. S., Nakamura, T., Inaguma, Y. and Itoh, M., Electronic transport phenomena of $La_{2/3+x}TiO_{3-\delta}$ ($x < 0.2$) metal–nonmetal transition by electron doping. *J. Solid State Chem.*, 1994, **113**, 281–299.
3. Abe, M. and Uchina, K., X-ray study of the deficient perovskite $La_{2/3}TiO_3$. *Mater. Res. Bull.*, 1974, **9**, 147–155.
4. Yashima, M., Mori, M., Kamiyama, T., Oikawa, K. I., Hoshikawa, A., Torii, S. *et al.*, High-temperature phase transition in lanthanum titanate perovskite $La_{0.64}(Ti_{0.92}\ Nb_{0.08})O_3$. *Chem. Phys. Lett.*, 2003, **375**, 240–246.
5. Battle, P. D, Bennet, J. E., Sloan, J., Tilley, R. J. D. and Ventle, J. F., A-site cation-vacancy ordering in $Sr_{1-3x/2}La_xTiO_3$: a study by HRTEM. *J. Solid State Chem.*, 1999, **149**, 360–369.
6. Ali, R. and Izumi, F., Neutron powder diffraction study of a phase transition in $La_{0.68}(Ti_{0.95}Al_{0.05})O_3$. *J. Am. Ceram. Soc.*, 2006, **89**, 3805–3811.
7. Yoshii, K., Synthesis and magnetic properties of $Ln_{2/3}TiO_3$ (Ln = Pr and Nd). *J. Solid State Chem.*, 2000, **149**(2), 354–359.
8. MacEachern, M. J., Dabkowska, H., Garrett, J. D., Amow, Gong, G. W., Liu, G. *et al.*, Metal–insulator transitions in $La_{1-x}TiO_3$ $0 \leq x \leq 0.33$. Structure–property correlation. *Chem. Mater.*, 1994, **6**, 2092–2102.
9. Sefat, A. S., Wu, M. Y., Botton, G. A. and Greedan, J. E., High-resolution EELS study of the vacancy-doped metal/insulator system, $Nd_{1-x}TiO_3$, $x = 0$ to 0.33. *J. Solid State Chem.*, 2005, **178**, 1008–1016.
10. Robertson, A. D., Garcia Martin, S., Coats, A. and West, A. R., Phase diagrams and crystal chemistry in the Li+ ion conducting perovskites, $Li_{0.5-3x}\ RE_{0.5+x}\ TiO_3$: RE = La, Nd. *J. Mater. Chem.*, 1995, **5**(9), 1405–1412.
11. Bian, J. J., Song, G. X and Yan, K., Structure and microwave dielectric properties of $Nd_{(2-x)/3}Li_xTiO_3$. *Ceram. Int.*, 2007, **34**, 893–896.
12. Skakle, J. M. S., Mather, G. C., Morales, M., Smith, R. I. and West, A. R., Crystal structure of the Li+ ion-conducting phases, $Li_{0.5-3x}RE_{0.5+x}\ TiO_3$: RE = Pr, Nd; $x = 0.05$. *J. Mater. Chem.*, 1995, **5**(11), 1807–1808.
13. Latie, L., Villeneuve, G., Conte, D., Flem and Le, G., Ionic conductivity of oxides with general formula $Li_xLn_{1/3}Nb_{1-x}Ti_xO_3$ (Ln = La, Nd). *J. Solid State Chem.*, 1984, **51**, 293–299.
14. Itoh, M., Inaguma, Y., Wu, J., Chen, L. and Nakamura, T., High lithium ion conductivity in the perovskite-type compounds $Ln_{1/2}Li_{1/2}TiO_3$ (Ln = La, Pr, Nd, Sm). *Solid State Ionics*, 1994, **70**, 203–207.
15. Harada, Y., Ishigaki, T., Kawai, H. and Kuwano, J., Lithium ion conductivity of polycrystalline perovskite $La_{0.67-x}Li_{3x}TiO_3$ with ordered and disordered arrangements of the A-site ions. *Solid state Ionics*, 1998, **108**, 407–413.
16. Ruiz, A. I., Lopez, M. L., Pico, C. and Veiga, M. L., Structural Modifications induced by composition in the $La_{1\,33-x}Na_{3x}Ti_2O_3$ perovskites: a neutron diffraction study. *Chem. Mater.*, 2005, **17**, 1391–1397.
17. Kim, J. S., Cheon, C. I., Kang, H. J., Lee, S. H., Kim, K. Y., Nam, S. *et al.*, Crystal structure and microwave dielectric properties of $CaTiO_3$-$(Li_{1/2}Nd_{1/2})TiO_3$-$(Ln_{1/3}Nd_{1/3})TiO_3$ (Ln = La, Dy) ceramics. *Jpn. J. Appl. phys.*, 1999, **38**(Pt 1), 9B.
18. Laguma, M. A., Sanjuan, M. L., Várez, A. and Sanz, J., Lithium dynamics and disorder effects in the Raman spectrum of $La_{(2-x)/3}Li_xTiO_3$. *Phys. Rev. B*, 2002, **66**, 054301.
19. Sanjuán, M. L., Laguna, M. A., Belous, A. G. and V'yunov, O. I., On the local structure and lithium dynamic of $La_{0.5}(Li\ Na)_{0.5}TiO_3$ ionic conductors. A Raman study. *Chem. Mater.*, 2005, **17**, 5862–5866.
20. Bian, J. J. and Yan, K., Structure and microwave dielectric properties of $La_{(2-x)/3}Na_xTiO_3$. *J. Electroceram.*, 2007, **21**(4), 132–136.